

Boundary Lubrication of PEO-PPO-PEO Triblock Copolymer Physisorbed on Polypropylene, Polyethylene, and Cellulose Surfaces

Y. Li,^{†,‡} O. J. Rojas,^{§,||} and J. P. Hinestrosa^{*,†}

[†]Department of Fiber Science and Apparel Design, Cornell University, Ithaca, New York 14853, United States

[§]Department of Forest Biomaterials, North Carolina State University, Campus Box 8005, Raleigh, North Carolina 27695-8005, United States

^{||}School of Chemical Technology, Department of Forest Products Technology, Aalto University, P. O. Box 16300, FI-00076 Aalto, Finland

ABSTRACT: In situ lateral force microscopy (LFM) and X-ray photoelectron spectroscopy (XPS) were used to probe the lubrication behavior of an aqueous solution of poly(oxyethylene)-poly(oxypropylene)-poly(oxyethylene) (PEO-PPO-PEO) symmetric triblock copolymer on thin films of polypropylene (PP), polyethylene (PE), and cellulose. LFM experiments were carried out while the substrates were immersed in water and in solutions of the copolymer. The friction coefficient on PP and PE was reduced after adsorption from the PEO-PPO-PEO aqueous solution while the opposite effect was observed for cellulose surfaces. A critical normal loading force, at which the friction coefficient of the lubricated and unlubricated surfaces is equal, was identified and related to the affinity of the polymer with the substrate. Further experiments were performed to mimic practical operations involving lubricant addition during manufacturing and postprocessing removal. XPS was used to verify the presence of the lubricant on the polymeric substrates and to evaluate its removal by water washing. The lubricant layer was easily removed by water from the PP and cellulose surfaces while a durable layer was found on PE. The XPS results were in agreement with the highest critical normal loading force measured for PE (52 nN for PE in contrast to a minimum of 10 nN for cellulose). While several reports exist on lubrication on hard surfaces, friction behavior on soft surfaces is still not well documented as the substrates usually deform under loading pressure. Therefore, we also propose a simple lubrication model for PP, PE, and cellulose and the use of critical normal loading force as a parameter to predict lubricity and durability of adsorbed nonionic block copolymers.

INTRODUCTION

During conventional textile and fiber manufacturing processes, lubricants are used to reduce friction on the fiber's surface and to prevent its abrasion. Textile lubricants are usually washed off after a fabric is manufactured either by woven, knit, or nonwoven processes. To be effective, lubricants must adhere well enough to the fibers to reduce friction during processing but be easily removed once the process is completed. In this paper we address lubricant adhesion and lubrication effectiveness on thin films of polymers commonly used in fiber and textile manufacturing.

Fiber lubrication can be divided into three categories depending on the gap between the fiber and the sliding surface: boundary lubrication, hydrodynamic lubrication, and semihydrodynamic lubrication.¹ According to the seminal work of Hansen and Tabor, boundary lubrication occurs at low sliding speeds and high contact pressures and in this regime the friction coefficient decreases with an increase of sliding speed, lubricant viscosity, and the reciprocal of pressure.¹ On the contrary, hydrodynamic lubrication occurs when there is large interfacial spacing and a continuous fluid film extends between two surfaces sliding at high speeds. The friction coefficient in the hydrodynamic lubrication increases with an increase in sliding speed, lubricant viscosity, and the reciprocal of pressure. Due to limitations in equipment accuracy to probe the boundary regime, studies on fiber lubrication have primarily focused on hydrodynamic lubrication.² As the layer of lubricant

in the hydrodynamic regime is thick and continuous, this regime is solely governed by the rheological properties of the lubricant.^{1,3} The transitional regime between the boundary and hydrodynamic lubrication is known as the semihydrodynamic regime.⁴

Boundary lubrication plays an important role in fiber processing, particularly when the fiber surface slides over other surfaces at slow relative speeds, and it has recently raised the interest of the scientific community from both fundamental and practical points of view.⁵ In the 1960s, Fort et al.⁶ studied the boundary regime on synthetic yarns using a conventional boundary friction apparatus. They found that lubricants with carboxylic polar groups significantly reduced friction on synthetic fibers by adsorbing as a thin monolayer onto the surface. This effect was not observed when working with nonpolar lubricants. More recently, boundary lubrication has been linked to process parameters, such as spinning velocity, normal pressure, and lubricant viscosity.^{3,7}

It is difficult to access boundary lubrication using friction measurement techniques. For example, the surface force apparatus (SFA) with tribology device and others require the surface to be very smooth. In contrast, textile materials often

Received: October 5, 2011

Revised: January 31, 2012

Accepted: January 31, 2012

Published: January 31, 2012



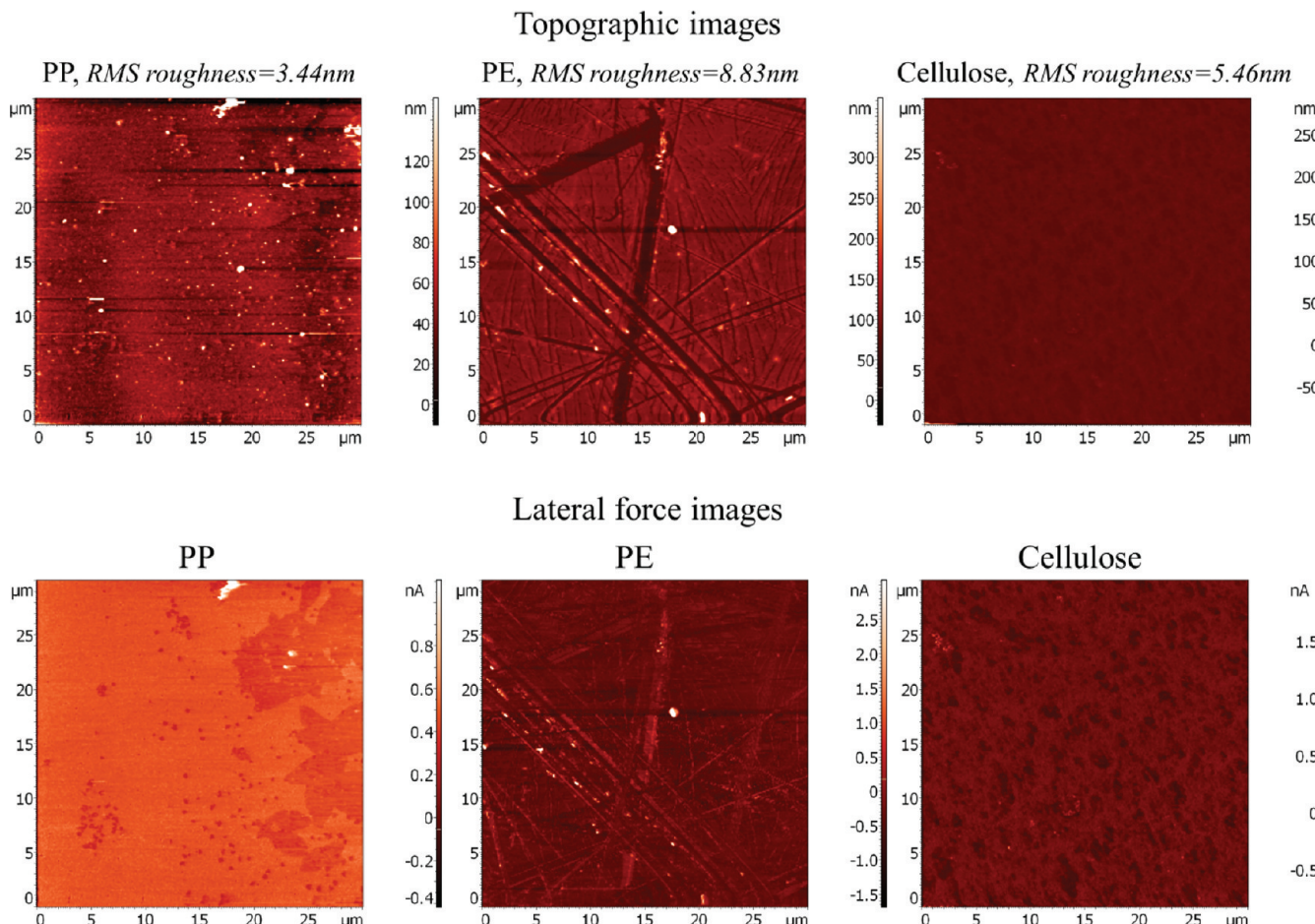


Figure 1. Topographic (top) and LFM (bottom) maps for PP, PE, and cellulose substrates imaged in air. The polymeric substrates appear smooth and flat but exhibit dissimilar friction response according to the LFM maps. These images were obtained using a loading force of 10.5 nN for PP, 11.2 nN for PE, and 10.7 nN for cellulose, respectively.

show relatively large roughness and heterogeneities in texture or chemical composition at the nanoscale. Furthermore, limited work has been done to correlate the chemical composition of lubricants and fibers with their lubrication behavior.⁸

Lubricants most commonly used in textile manufacturing are composed of fatty acids, mineral oils, ethoxylated acids, and silicones.⁹ These lubricants can be cationic, anionic, or nonionic.¹⁰ Recently, nonionic surfactants have been of great interest due to their numerous advantages, including good solubility in water and organic solvents, compatibility with most surfactants, and availability as electrolyte-free material.¹¹ Poly(oxyethylene)-poly(oxypropylene)-poly(oxyethylene) (PEO-PPO-PEO; Pluronic) triblock copolymer is a nonionic surfactant consisting of two hydrophilic PEO blocks and a hydrophobic PPO block.¹² The molecular weight and the PEO/PPO ratio of these surfactants can be adjusted to tailor their properties as lubricants, texturizers, softeners, emulsifiers, dispersers, and antistatic and wetting agents.¹³ Pluronic copolymers have high wetting and spreading ability, allowing them to form uniform coatings on textiles that can result in low friction, antistatic properties, dye-leveling improvement, and easy cleaning.¹³

Analytical techniques such as optical ellipsometry,¹⁴ total internal fluorescence spectroscopy (TIRF),¹⁵ surface plasmon resonance (SPR) spectroscopy,¹⁶ and atomic force microscopy (AFM)¹⁷ have been employed to probe molecular structures

formed on a number of surfaces by the hydrophilic and hydrophobic blocks of copolymers. For example, Marques et al. first proposed a so-called buoy–anchor–buoy model of triblock copolymers to explain their adsorption on polymer surfaces.¹⁸ They correlated chemical compositions with the molecular self-assembled structures formed on the surface. It was proposed that the hydrophobic PPO blocks strongly bind to the surface forming a thin layer, while the hydrophilic PEO blocks dangle from the surface, extending into the liquid and forming a free “brush” layer. Zhang and Archer reported that when the packing density in the lubricant layers was kept constant, a self-assembled monolayer containing both short and long polymer chains provided lower friction coefficients and improved wear resistance when compared with single-component self-assembled monolayers.¹⁹

Lateral force microscopy (LFM; or friction force microscopy, FFM) has been employed to probe molecular structures on hard substrates at micro- and nanoscales.^{20–22} For example, LFM was used to determine that self-assembled perfluoroctyl-trichlorosilane (FOTS) and octadecyltrichlorosilane (OTS) monolayers unfolded into different molecular configurations when deposited onto silica wafers.²³ While FOTS had a rigid rodlike helical structure, OTS had a zigzag backbone configuration, offering different lubrication performance. Friction anisotropy and asymmetry were also discovered via LFM of monolayers of polydiacetylene.^{24,25} The surfaces in

these studies were mica,²⁶ silica,²⁷ and graphite.²⁸ Polymer and fiber surfaces are quite different as they are soft, deformable, and highly energy-dissipative. Thus, the study of boundary lubrication on fiber and polymer surfaces is more complex.²⁹

In this paper thin films of three polymers commonly made into fibers, namely, polypropylene (PP), polyethylene (PE), and cellulose, were spin-coated on silica wafers. Solutions of the triblock copolymer EO₁₉PO₂₉EO₁₉ were applied to the polymeric substrates, and their lubrication behavior was examined using *in situ* LFM. The strength of lubricant attachment on the surfaces was confirmed and further assessed using X-ray photoelectron spectroscopy (XPS). These findings may provide a new framework for the formulation of lubricants and the prediction of their lubrication performance on deformable surfaces.

EXPERIMENTAL SECTION

Preparation of Model Surfaces. Polymeric surfaces were prepared following the procedure reported by Song et al.³⁰ Briefly, 20 mg of PE ($M_n \approx 1110$; $M_w/M_n \approx 1.11$; Sigma Aldrich) or PP ($M_n \approx 5000$; $M_w/M_n \approx 2.4$; Sigma Aldrich) were dissolved in 10 mL of xylene. The solutions were stirred for more than 2 h under a condensation system. Silica wafers (Wafer World, West Palm Beach, FL, USA) were washed with a H₂SO₄:H₂O₂ (70:30) solution and cleaned by ultraviolet–ozone (UVO) treatment. An IR lamp was used to heat the surfaces and pipettes to a temperature of 85 °C. One or two drops of PE or PP solution were spin-coated onto the cleaned silica wafer at 2000 rpm for 20 s using a WS-400A-6NPP spin coater (Laurell Technologies). Samples were placed in an oven at 80 °C to evaporate residual solvent. XPS was used to determine that the films were free of any residual solvent.

To prepare cellulose surfaces, a modification after Gunnars' method was followed:³¹ Clean silica wafers were immersed in poly(vinyl amide) (PVAm, BASF) aqueous solution (100 ppm) for 20 min. The PVAm-coated surface was washed with milli-Q water to remove excess PVAm and dried with nitrogen. PVAm was used as an anchoring polymer to bind cellulose to the silica wafers. To prepare cellulose solutions, 50 mg of microcrystalline cellulose (Avicel) was added to a 2.5 mL N-methylmorpholine-N-oxide (NMMO) solution (50 vol %). The solution was heated and stirred at 115 °C. After the solution became transparent, 7.5 mL of dimethyl sulfoxide (DMSO) was added to adjust the viscosity. A drop of the cellulose solution was filtered through a disk-filter and spin-coated at 5000 rpm onto the PVAm-coated silica wafers.

Figure 1 shows the polymer thin films on the silica wafers as imaged in air via LFM. The topographic and lateral force images were obtained simultaneously. The scanning area is 30 μm × 30 μm. The topographic images (Figure 1a) show uniform PP and cellulose thin films while the PE film featured linear fractures. The root-mean-square (rms) surface roughness calculated on the 30 μm × 30 μm images was determined to be less than 10 nm. LFM images are shown as lateral force images (Figure 1b). Although the PP and cellulose surfaces exhibit topographic uniformity, their friction properties appear to be spatially dependent. On the other hand, the LFM image of the PE surface appears similar to the topographical image. Differences in topographical and frictional maps have been attributed to differential crystallization kinetics.³²

Polymer Solutions. An aqueous 1% by weight solution of EO₁₉PO₂₉EO₁₉ (obtained from BASF) was prepared. This concentration value is above the critical micelle concentration

(cmc) reported for this amphiphilic polymer (10⁻⁵ to 10⁻³% by weight).³³ Solutions of this type are employed as lubricants in various processing technologies, and thus, for simplicity, they are also referred to as "lubricant solution" or "lubricant" in the following discussion.

X-ray Photoelectron Spectroscopy Analysis. XPS spectra were acquired using a Surface Science Instrument SSX-100 X-ray photoelectron spectrometer employing monochromatic Al K α X-rays at 1486.6 eV at an operating pressure < 2 × 10⁻⁹ Torr. Photoelectrons were collected at an angle of 55° from the surface. Pass energies of 150 and 50 V were used for survey and high-resolution C1s scans. For XPS analysis, the specimens were probed under three different conditions: (a) pristine substrate surface deposited on a silica wafer, (b) substrate after adsorption of EO₁₉PO₂₉EO₁₉ from aqueous 1 wt % solution (after 24 h adsorption equilibrium), and (c) specimens from b after washing with DI water and 95% ethanol, and dried with a gentle jet of compressed and filtered air.

Lateral Force Microscopy. An atomic force microscope (NTEGRA Prima, NT-MDT, Zelenograd, Russian Federation) was employed to probe the frictional properties of the model polymer surfaces under three different conditions. LFM measurements were conducted in air (air test), while the sample was submerged in DI water (water test), and while immersed in a 1% by weight lubricant solution (lubricant test). A Mikro Masch contact mode probe with a force constant of 0.35 N/m was used. In both immersion tests (water test and lubricant test), the solution was injected into a liquid metal cell in which the wafer samples were positioned. All of the tests were performed with a scan frequency of 1 Hz. During LFM, samples were scanned in a direction perpendicular to the long axis of the probing cantilever. Friction values were recorded using line profiles on the sample surface in three scanning conditions (in air, in water, and in lubricant solution). The scanning size was 5 μm × 5 μm, suggesting that the line profile of lateral force was based on 5 μm.

In LFM, lateral line scans provide information about both friction distribution and surface topography. To examine friction forces, the topographical effect needs to be decoupled from the tribological effect. In one forth and back scan loop, the values of frictional force change in sign while the sign for the normal load remains the same. By subtracting the forth and back images, one obtains the double of the frictional force while eliminating the influence of surface topography. Therefore, the friction forces can be obtained by dividing by two the sum of the lateral force values from the forth scan and the back scan. Lateral force values were converted from current (LAT) through the relation

$$F_l = \frac{l^2}{4l_{tip}LBc} LAT \quad (1)$$

where F_l is the friction force, l is the length of the cantilever, l_{tip} is the length of the tip, L is the distance between the mirror and the photodiode, B is the calibration constant, $1/c$ is the spring constant of the cantilever, and LAT is the recorded lateral force signal. B is determined by a traditional calibration procedure that is unique to each AFM manufacturer.

The normal loading forces F_n were determined using the method reported by Liu et al.³⁴ The applied load was varied from 5.5 to 75 nN. Five replicates of line profiles were independently performed for different locations on the surfaces

in order to determine the standard deviation of the measurements.

RESULTS AND DISCUSSION

Friction Coefficients. When an AFM tip slides across a surface under a total loading normal force F , it will be deformed both in the vertical and horizontal directions. The force normal to the surface (F_n) bends the free end of the cantilever in the vertical direction, while simultaneously the force parallel to the surface (F_l) twists the cantilever in the horizontal direction. The friction coefficient is given by the ratio of F_l to F_n .

Polypropylene. Friction coefficient curves of the polypropylene thin films as a function of applied normal force under three different experimental conditions can be observed in Figure 2

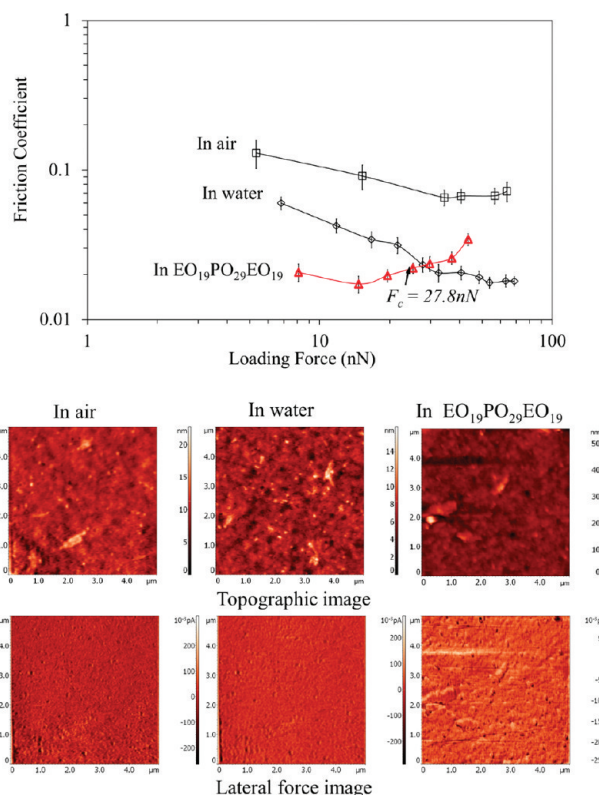


Figure 2. Friction coefficient curves as a function of loading normal force for a PP substrate under three different imaging conditions (in air, immersed in water, and immersed in an $\text{EO}_{19}\text{PO}_{29}\text{EO}_{19}$ aqueous solution) and the corresponding lateral force images. The curves indicate the presence of a critical normal loading force at which the coefficient of friction measured in water is equal to the one measured while the sample is immersed in $\text{EO}_{19}\text{PO}_{29}\text{EO}_{19}$ aqueous solution. This crossover point appears to indicate the maximum loading force at which the block copolymer solution may exhibit lubrication behavior. Uniform and featureless structures are seen when the samples are imaged in air and in water, but a LFM image with some granular features is seen for the lubricated PP surface reflecting the presence of the lubricant coating on its surface. These images were obtained at loading force of 5.1 nN for the condition in air, 6.5 nN for the condition in water, and 8.2 nN for the condition in lubricant solution, respectively.

along with the corresponding lateral force images. The friction coefficients measured in air and in water appear to decrease with increasing loading (normal) forces in sharp contrast to the behavior of hard surfaces such as gold, mica, and graphite.³⁵ A

decrease in friction coefficient with increasing loading force reflects a different physical response exhibited by these deformable polymers. This observation was discussed by Wong and Granick who speculated that when polymers are subject to sliding contact forces, the normal pressure is reduced due to the deformability of the substrate and thus the coefficient of friction is also reduced.³⁶

The values for friction coefficient for the PP substrate when probed in water were lower than those measured when the sample was scanned in air. This behavior was expected as imaging in water reduces capillary forces between the tip and the substrate.³⁷ When the PP surface was immersed in the lubricant solution, the friction coefficients were further reduced compared with those measured in water, suggesting that the triblock copolymer $\text{EO}_{19}\text{PO}_{29}\text{EO}_{19}$ forms a lubricant layer covering the PP surface. Another indication of the presence of a lubricant layer is the lateral force image which shows some granular features. It is particularly important to note that as loading force increases, the friction coefficient slowly increased and when the loading force reached 27.8 nN, the friction coefficients of the lubricated polymer were equal to that in water. We called this crossover value the critical normal loading force. It is proposed that at the critical normal loading force damage to the lubricant layer begins, destroying their layering structures and preventing them from functioning as an effective lubricant.

Polyethylene. Figure 3 shows the friction coefficient curves as a function of normal loading force as well as lateral force images of a polyethylene specimen while probed in air, immersed in water, and submerged in lubricant solutions of $\text{EO}_{19}\text{PO}_{29}\text{EO}_{19}$. The PE friction curves reflect behavior similar to those of PP with the presence of a crossover critical normal loading force of 51.7 nN. A granular frictional map is observed on the PE LFM image when it is obtained in air. These granular features become blurred when the specimen is imaged in water, but they appear again, although exhibiting smaller characteristic features when the sample was imaged immersed in the $\text{EO}_{19}\text{PO}_{29}\text{EO}_{19}$ aqueous solution. These changes in the frictional map are evidence of the presence of a lubricant layer on the surface of the PE specimen. At values above the critical normal loading force, the self-assembled structure of the lubricant appears to break down, hence decreasing their lubrication characteristics as reflected by a sudden increase in the friction coefficient. The critical normal loading force is almost twice as large for the PE specimen than for the PP sample. This difference is an indication of the preferred affinity of the $\text{EO}_{19}\text{PO}_{29}\text{EO}_{19}$ toward the PE surface which was recently verified and quantified via molecular dynamic simulations.³⁷

Cellulose. The relationships between friction coefficient and loading normal force for the cellulose surface scanned under three different environments are shown in Figure 4. The friction coefficient curves indicate that when the cellulose specimen is imaged in water, the friction coefficient decreases in a manner similar to that observed on PP and PE surfaces. However, with the addition of the lubricant solution, a significantly different behavior was observed: the friction coefficients obtained when the sample was probed in lubricant solution were higher than those measured in water, across the full range of loading forces applied. In addition, no crossover point was observed. This unique behavior can be explained by the presence of a loosely attached lubricant layer, so the crossover critical normal loading force occurred at lower loading forces than the ones measured (<10 nN). Lateral force

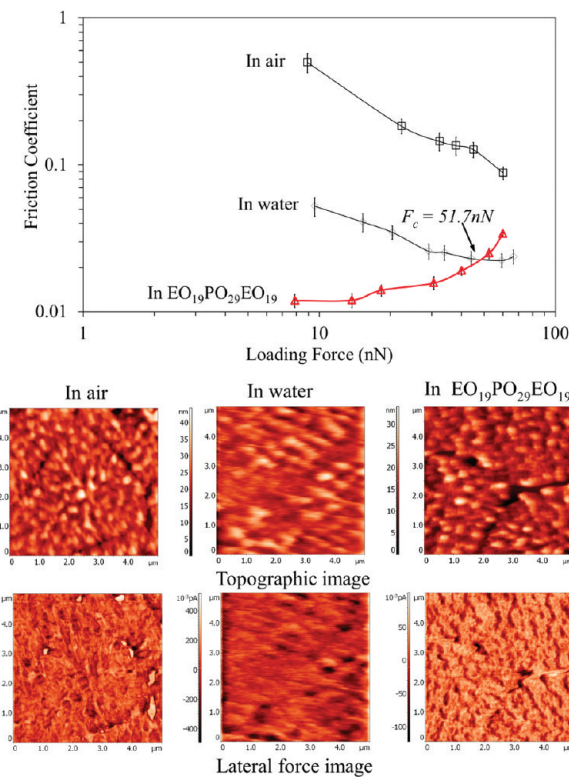


Figure 3. Friction coefficient curves as a function of loading normal force for a PE specimen imaged under three different conditions (in air, immersed in water, and submerged in EO₁₉PO₂₉EO₁₉ aqueous solution). The corresponding LFM images are also included. Lateral force images indicate frictional maps that depend on the imaging environment, and the friction coefficient curves reveal the presence of a critical normal loading force. There images were obtained at loading force of 8.8 nN for imaging in air, 9.5 nN for imaging in water, and 7.8 nN for imaging in lubricant solution, respectively.

imaging revealed very little difference between the image obtained while the sample was immersed in water and the one obtained when the sample was immersed in the lubricant solution confirming that the EO₁₉PO₂₉EO₁₉ can be easily removed from the cellulose surface.

Surface Chemical Composition and Lubricant Durability. In textile and fiber manufacturing, lubricants are applied during processes such as spinning, carding, drafting, weaving, knitting, and many others. Lubricants are introduced with the main purpose of reducing friction and preventing fiber surfaces from abrasion damage. It is customary that after the fibers or fabrics have been processed, the final textile products need to be clean and free of any textile finishes and lubricants. The removal of these lubricants is usually achieved by washing the finished product with water. XPS was used to determine the surface chemical composition and therefore to assess the resistance to removal by washing of the lubricant layer, i.e., to evaluate the durability of the lubricant adsorbed onto the substrate.

Polyethylene. Figure 5 shows survey XPS spectra for the PE specimen under three different conditions: Pristine polyethylene substrate (PE), PE after the EO₁₉PO₂₉EO₁₉ lubricant was applied (PE + lubricant), and PE after the lubricated specimen was washed with water (PE + lubricant + washing). The relative surface atom percent (C, O, and Si composition from C1s, O1s, and Si1s signals, respectively) were obtained from the XPS photoelectron intensities at the respective

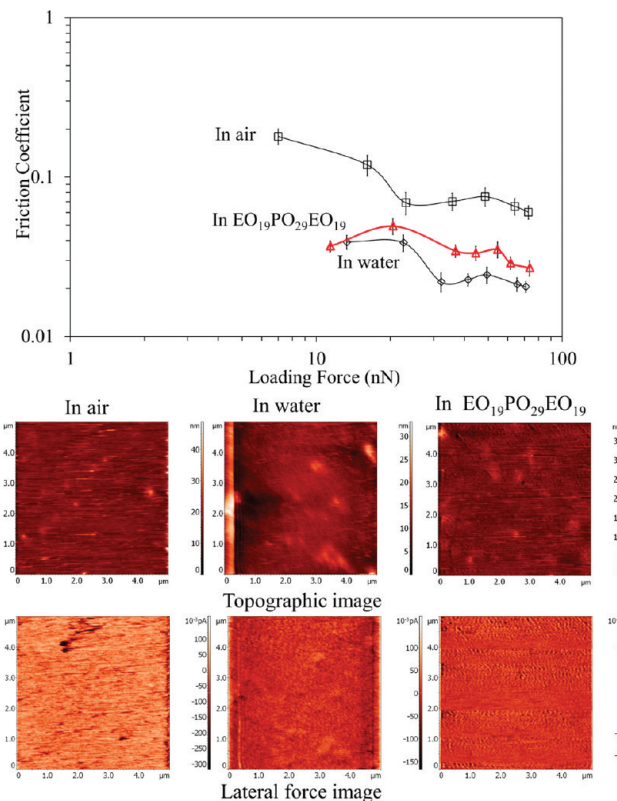


Figure 4. Friction coefficients of a cellulose surface as a function of normal loading force along with corresponding frictional mapping obtained via LFM under three imaging conditions: sample in air, sample immersed in water, and sample submerged in EO₁₉PO₂₉EO₁₉ aqueous solution. The absence of a crossover point as well as the similarities of the LFM images obtained when the sample was submerged under water and in lubricant solutions appear to indicate that the EO₁₉PO₂₉EO₁₉ is loosely attached to the cellulose surface. For this particular substrate, water has a more beneficial effect on the lubrication of the cellulose surface than that of the EO₁₉PO₂₉EO₁₉ aqueous solution. There images were obtained at loading force of 7.1 nN imaging air, 10.3 nN for imaging in water, and 10.4 nN for imaging in lubricant solution.

binding energies (see XPS survey spectra in Figure 5). For PE, the elemental analysis shows 96% of carbon which is close to the theoretical composition of the polymer and small percentages of oxygen (2%) and silicon (1%). PE does not contain any O or Si, so these signals originated from the oxidized silicon substrate underneath the layer of spin-coated PE. Song et al. reported that the thickness of the PE layer was in the range of 20–50 nm when the same surface preparation method was used.³⁰ Therefore, the presence of the Si and O peaks indicates some patches on the surface where the thickness of the polymer layer is reduced to 10 nm, which is the penetration depth in XPS analyses.³⁸ For the PE + lubricant specimen a larger O1s peak was observed in the survey spectra and the percentage of O was significantly increased by an order of magnitude (to ca. 28% while the signal for Si was below the XPS detection limit).

The percent values for C and O for the PE + lubricant specimen are between the theoretical figures calculated for EO₁₉PO₂₉EO₁₉ lubricant and those for pure PE substrate, indicating that the layer of lubricant completely covers the PE substrate and that the thickness of the lubricant layer on top of the PE is less than 10 nm. Once the sample is washed with

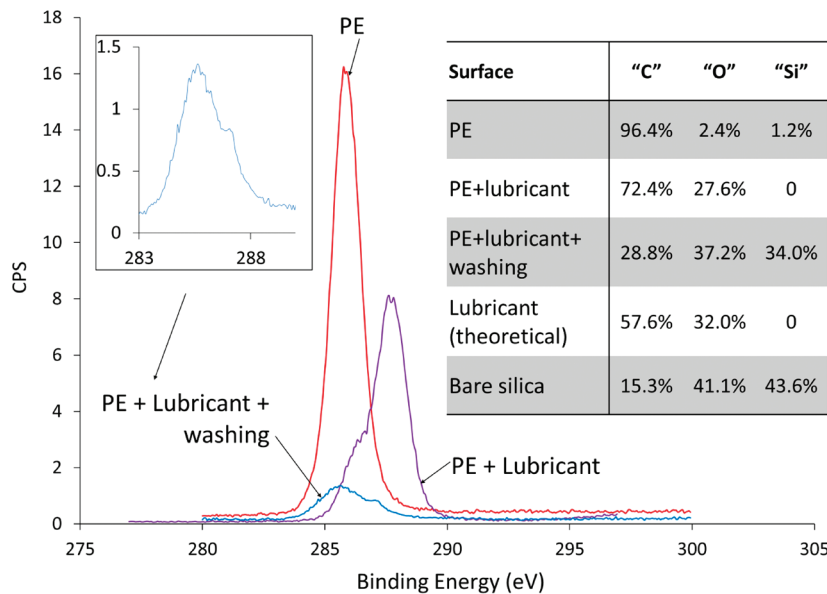


Figure 5. XPS survey spectra and relative elemental analysis for PE specimens probed under three different conditions: pristine PE and PE surface after the $\text{EO}_{19}\text{PO}_{29}\text{EO}_{19}$ lubricant was applied (P + lubricant) and after the lubricated surface was washed with water (PE + lubricant + washing). After the lubricant was applied on the PE substrate, a decrease of the C1s peak, an increase of the O1s peak, and the absence of a Si1s peak (PE + lubricant) indicate that the lubricant completely covered the PE. After washing, the film was dewetted from the silica surface, and, due to the strong binding of the lubricant layer to the PE substrate, most of the lubricant was removed (PE + lubricant + washing).

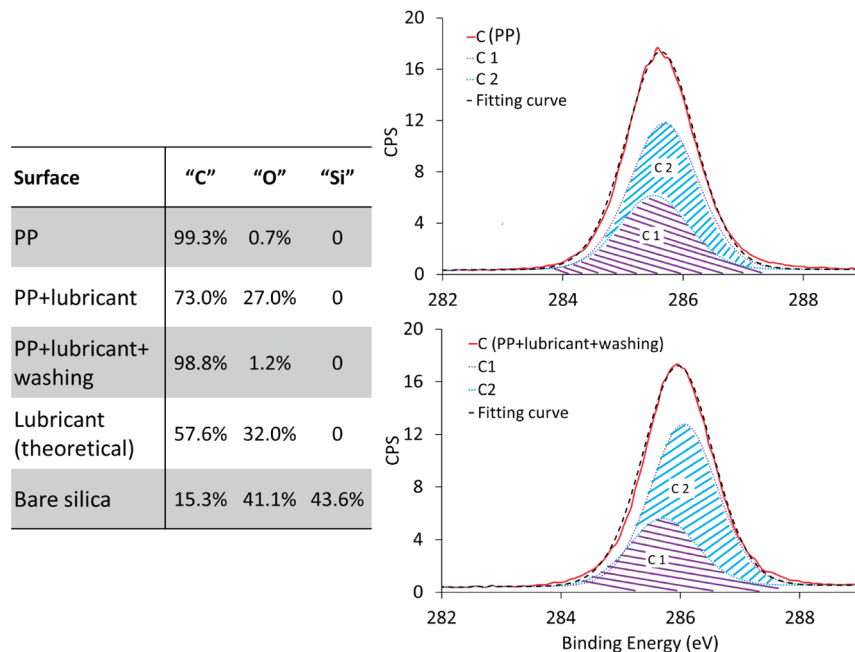


Figure 6. XPS relative atom percent composition (table on the left) for PP samples: pristine polypropylene surface (PP) and PP surface after the $\text{EO}_{19}\text{PO}_{29}\text{EO}_{19}$ lubricant was applied (PP + lubricant) and after the lubricated surface was washed with water (PP + lubricant + washing). The C1s carbon spectra (right) correspond to pristine PP sample (top) and the PP + lubricant + washing sample (bottom). The shadowed peaks are obtained after deconvolution of signals from C1 at 285.5 eV (purple) and in C2 at 285.7 eV (blue). The similarity of the PP and PP + lubricant + washing deconvolution curves for C1s as well as the relative elemental analysis indicate that the lubricant was able to completely cover the PP surface and after washing with water, the lubricant layer was effectively removed.

water, the XPS survey spectrum indicates a large percentage of Si, suggesting the dewetting of the PE substrate from the silica wafer. It is also reported that some of the pure PE coating could be also washed off due to dewetting phenomenon.^{39,40} However the O/Si ratio for the washed sample (1.09) is larger than the O/Si for the bare silica (0.9). This difference shows that there were some PE and lubricant remaining on the surface

after washing, and it also may provide indirect evidence that the $\text{EO}_{19}\text{PO}_{29}\text{EO}_{19}$ lubricant was strongly attached to the PE surface so that it was removed simultaneously with the PE layer during the washing process. This behavior is opposite to that exhibited by the polypropylene and cellulose substrates to be discussed below.

Surface	"C"	"O"	"Si"
Cellulose	58.5%	40.0%	1.5%
Cellulose +lubricant	72.8%	27.2%	0
Cellulose +lubricant +washing	55.8%	39.5%	4.7%
Lubricant (theoretical)	57.6%	32.0%	0
Bare silica	15.3%	41.1%	43.6%

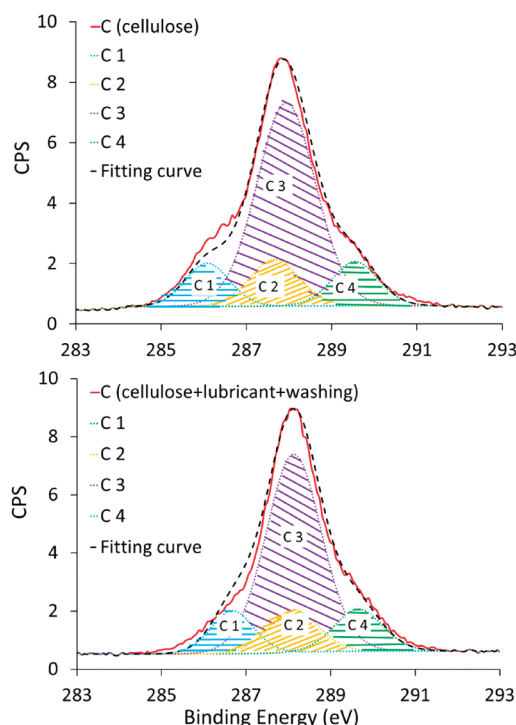


Figure 7. XPS relative atom percent composition (table on the left) for a cellulose specimen under three different conditions (right): pristine cellulose surface (cellulose) and after the $\text{EO}_{19}\text{PO}_{29}\text{EO}_{19}$ lubricant was applied (cellulose + lubricant) and after the lubricated surface was washed with water (cellulose + lubricant + washing). The C1s carbon spectra (right) correspond to the pristine cellulose sample (upper) and the cellulose + lubricant + washing sample (lower). The shadowed peaks are obtained after deconvolution, corresponding to the carbon in C1 at 286.1 eV (blue), in C2 at 287.7 eV (yellow), in C3 at 287.7 eV (purple), and in C4 at 289.5 eV (green). According to the relative elemental analysis, the lubricant was able to completely cover the cellulose surface and further deconvolution of the C1s peaks into the four cellulose C1s types indicates that the lubricant layer was effectively removed from the cellulose surface after washing.

Polypropylene. Figure 6 illustrates the XPS survey spectra as well as the elemental analysis for PP experiments performed under three different conditions: Pristine polypropylene substrate (PP), PP substrate after the $\text{EO}_{19}\text{PO}_{29}\text{EO}_{19}$ lubricant was applied (PP + lubricant), and PP substrate after washing with water (PP + lubricant + washing). The magnitude of the peak for the PP + lubricant + washing specimen is significantly higher than that for the PE + lubricant + washing, indicating that the layer of PP survived the washing conditions. The atom percent composition indicates that the pristine PP specimen spun onto the silica wafer has a thickness higher than 10 nm as no signal from silicon is detected and a negligible amount of oxygen is noted. After the sample was immersed in the lubricant and dried, XPS shows an increase in the percentage of oxygen, indicating the presence of an $\text{EO}_{19}\text{PO}_{29}\text{EO}_{19}$ layer. However the percentage of oxygen detected was lower than the theoretically expected value for an $\text{EO}_{19}\text{PO}_{29}\text{EO}_{19}$ which can be interpreted as evidence that the XPS beam penetrated to the PP layer. After the specimen was washed, the elemental atom percent carbon and oxygen returned to values closer to those of the PP surface while the silicon signal was below the detection limit of the instrument. These values are indicative that only the lubricant layer was washed away. These observations are in agreement with a lower value for the critical normal loading force value determined via LFM for the PP system. The deconvolution of the carbon peak for the PP and the PP + lubricant + washing specimens showed negligible changes in the areas for the two types of carbon (C1 at 285.5 eV and C2 at 285.7 eV, respectively) present in the PP structure, hence

confirming that the lubricant has been effectively removed during the washing procedure.

Cellulose. Figure 7 shows a C1s XPS detailed spectra for the cellulose films. Cellulose is a more complex molecule than PP and PE, and the presence of three different carbon atoms and oxygen further complicates the analysis of the spectra. The samples probed consisted of pure cellulose (cellulose); cellulose substrates after $\text{EO}_{19}\text{PO}_{29}\text{EO}_{19}$ lubricant was applied (cellulose + lubricant); and cellulose substrates after the lubricated sample was washed with water (cellulose + lubricant + washing).

The elemental analysis shows that the O/C ratio, 0.68 for pristine cellulose surface, is found to be comparable with the O/C ratio reported for cellulose filter paper reported by Carlsson and Stroem.⁴¹ It is found that the pristine layer of cellulose deposited over the silica wafer is smaller than 10 nm as traces of Si are detected. After the lubricant is applied, the Si signal disappears and the percentage of oxygen decreases as an indication of the presence of the $\text{EO}_{19}\text{PO}_{29}\text{EO}_{19}$ lubricant. After the specimen is washed, the percentages of carbon and oxygen return to values similar to those of the pristine cellulose surface and a small signal for Si is again detected. The percentage for Si is larger for the washed sample than for the pristine cellulose specimen, indicating that a small amount was desorbed. Dorris et al. used XPS to analyze the carbon peak of cellulose and suggested the carbon peak was composed of four types of carbon peaks.⁴² Deconvolution of the carbon peak into four different carbons (C1 at 286.1 eV, C2 at 287.7 eV, C3 at 287.9 eV, and C4 at 289.5 eV, respectively) indicate negligible changes or shifts in binding energy between the cellulose sample and the washed specimen, corroborating that the

lubricant was effectively removed during the washing procedure. These observations also corroborate the findings obtained via LFM and discussed in earlier sections of this paper.

In summary, $\text{EO}_{19}\text{PO}_{29}\text{EO}_{19}$ was easily removed from the PP and cellulose surfaces after rinsing and drying. In contrast, traces of the lubricant remained on the PE surface after rinsing. These observations confirm that the interaction of the $\text{EO}_{19}\text{PO}_{29}\text{EO}_{19}$ lubricant with the PE surface is stronger than that with the PP and cellulose surfaces, in agreement with conclusions drawn from the critical loading force data in the LFM analysis.

Proposed Lubrication Mechanism on PP, PE, and Cellulose Surfaces. According to the LFM experiments, $\text{EO}_{19}\text{PO}_{29}\text{EO}_{19}$ acts as a lubricant for the PE and PP surfaces but not for the cellulose surface. These results highlight that the molecular interaction of the triblock copolymer with the polymeric surfaces plays a key role on the adsorption process and the strength of the lubricant layer. In $\text{EO}_{19}\text{PO}_{29}\text{EO}_{19}$, the EO block is hydrophilic in nature while the PO block is hydrophobic. The block PPO has higher affinity for hydrophobic surfaces such as PE and PP than for hydrophilic cellulose.⁴⁴ Figure 8 shows schematically how the triblock

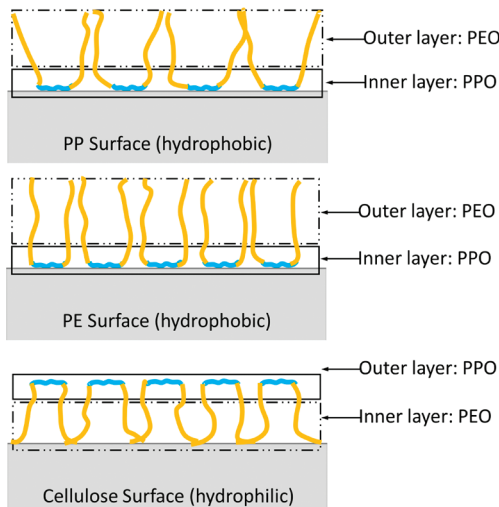


Figure 8. Schematic diagram illustrating a proposed model on how a triblock copolymer such as $\text{EO}_{19}\text{PO}_{29}\text{EO}_{19}$ may coat hydrophobic and hydrophilic surfaces. On the PP (a) and PE (b) surfaces the outer layer is composed of the flexible PEO chains while the inner layer of PPO blocks anchors the copolymer to the surface. The exposed flexible PEO blocks enhance the lubrication of the surface while, on the hydrophilic cellulose surface (c), the PEO blocks of the copolymer adhere to the surface, exposing the PPO block and hindering lubrication.

copolymer is expected to interact with the PP, PE, and cellulose surfaces. On the PP and PE surfaces the PPO blocks of the lubricant have higher affinity for the surface, and they anchor to it, forming a well-packed inner layer. Above the inner layer, there is an outer layer with soft PEO blocks that dangle outward from the solid surface. The flexible polymer hairs of the outer layer behave like a liquid and lubricate the surface.^{19,43} Similar configurations have previously been described as buoy-anchor–buoy (B–A–B) structures which are formed by PPO-PEO-PPO triblock copolymers in aqueous solutions on hydrophobic polymeric surfaces such as polystyrene (PS) and poly(dimethylsiloxane) (PDMS).^{44,45} The reduction in friction

observed on polymer surface lubricated by a series of PPO-PEO-PPO triblock copolymers has also been reported by Lee et al.⁴⁶

The inner PPO layer on the PP and PE surfaces is well-packed and effectively prevents penetration of the surface, resulting in protection of the surface and hence a higher critical normal loading force. The exposed polymer hairs are known to provide lubrication. There are several examples in the literature where a similar friction reduction is observed in surfaces with extending flexible polymeric chains. One example is a PS/PDMS diblock copolymer deposited on polystyrene surfaces. In this copolymer layer, the PS block penetrates the PS surfaces leaving flexible PDMS tails outstretched from the surfaces functioning as a lubricating layer.⁴⁵ Hydrogels with brushlike dangling chains have also been reported to produce better lubrication than those without such flexible chains on their surfaces.^{47,48} If the upper layers are crossed-linked, the networks with larger average length between adjacent crossed-linked points are more flexible and thus decrease the friction coefficient to a higher degree than those having tight cross-linking structures. This behavior is usually attributed to the mobility of the polymer chains.⁴⁹ In contrast with the PP and PE surfaces, the PEO block has a higher affinity with cellulose than the PPO block so a reversed structure of the anchor–buoy–anchor (A–B–A) is proposed. The PEO blocks are expected to anchor to the hydrophilic cellulose surface while the PPO blocks are away from the hydrophobic surface.¹⁷ Thus, the outer layer of PPO blocks has far less flexibility, and this lack of flexibility is reflected in higher friction coefficient.

CONCLUSIONS

Lateral force microscopy was used to provide insights on the adsorption and lubrication behavior of a symmetric $\text{EO}_{19}\text{PO}_{29}\text{EO}_{19}$ triblock copolymer. It was found that adsorbed $\text{EO}_{19}\text{PO}_{29}\text{EO}_{19}$ reduced friction on polypropylene and polyethylene, but it was not an effective lubricant for cellulose. The existence and magnitude of a critical normal loading force appears to correlate with the ability of the lubricant to attach to the substrate. This parameter may be used in the future to predict the behavior of lubricants on polymeric materials of industrial relevance. Furthermore, LFM data indicated that lubrication on soft materials may be a significantly different phenomena than that on hard and nondeformable surfaces and that the coefficient of friction is a strong nonlinear function of the applied normal force.

XPS was used to evaluate the strength of affinity of the lubricant layer with the substrate solution. A model describing the configuration of $\text{EO}_{19}\text{PO}_{29}\text{EO}_{19}$ on the cellulose, polyethylene, and polypropylene surfaces was proposed to explain the lubrication behavior observed via LFM. In the proposed model, flexible PEO polymer chains dangle away from the hydrophobic surfaces and may act like a liquid-enhancing lubricant while the anchoring of these brushes to the hydrophilic surface increases friction. The results provide a new perspective toward understanding complex lubrication phenomena on soft and deformable materials of industrial relevance.

AUTHOR INFORMATION

Corresponding Author

*Tel.: +1-607 255 7600. Fax: +1-607 254 1291. E-mail: jh433@cornell.edu.

Present Address

[‡]The KAUST-Cornell Center for Energy and Sustainability, Cornell University, Ithaca, NY, 14850.

Notes

The authors declare no competing financial interest.

ACKNOWLEDGMENTS

This work was supported by the National Textile Center under Grant No. C05-NS09. Junlong Song is acknowledged for help in preparing the polymeric substrates. Y.L. thanks Prof. Lawrence M. Cathles (Earth and Atmospheric Science, Cornell University) for giving priceless help in discussing the paper and for English guidance.

REFERENCES

- (1) Hansen, W. W.; Tabor, D. Role of Hydrodynamic Lubrication in the Friction of Fibers and Yarns. *J. Appl. Phys.* **1956**, *27*, 1558–1559.
- (2) Schick, M. J. Friction and Lubrication of Synthetic Fibers Part VII: Effect of Guide Temperature. *Text. Res. J.* **1980**, *50* (11), 675–681.
- (3) Schick, M. J. Friction and Lubrication of Synthetic Fibers Part IV: Effect of Fiber Material and Lubricant Viscosity and Concentration. *Text. Res. J.* **1973**, *43* (6), 342–347.
- (4) Olsen, J. S. Frictional Behavior of Textile Yarns. *Text. Res. J.* **1969**, *39* (1), 31–37.
- (5) Gupta, B. S., Ed. *Friction in Textile Materials*; Woodhead: Philadelphia, PA, USA, 2008.
- (6) Fort, T.; Olsen, J. S. Boundary Friction of Textile Yarns. *Text. Res. J.* **1961**, *31* (12), 1007–1011.
- (7) Schick, M. J. Friction and Lubrication of Synthetic Fibers Part I: Effect of Guide Surface Roughness and Speed on Fiber Friction. *Text. Res. J.* **1973**, *43* (2), 103–109.
- (8) Behary, N.; Campagne, C.; Caze, C.; Perwuelz, A. Using an Electronic Microbalance Technique to Study the Stick-Slip Behavior of Lubricated Polypropylene Fibers. *J. Appl. Polym. Sci.* **2003**, *89* (3), 645–654.
- (9) Postman, W. Spin Finishes Explained. *Text. Res. J.* **1980**, *50* (7), 444–453.
- (10) Briscoe, B. J.; Motamedi, F. Role of Interfacial Friction and Lubrication in Yarn and Fabric Mechanics. *Text. Res. J.* **1990**, *60* (12), 697–708.
- (11) Rosen, M. J. *Surfactants and Interfacial Phenomena*, 3rd ed.; John Wiley and Sons: New York, 2004.
- (12) Yu, G.; Deng, Y.; Dalton, S.; Wang, Q.; Attwood, D.; Price, C.; Booth, C. Micellisation and Gelation of Triblock Copoly(oxyethylene/oxypropylene/oxyethylene), F127. *J. Chem. Soc., Faraday Trans.* **1992**, *88*, 2537–2544.
- (13) Schmolka, I. R. Block Polymer Nonionic Surfactants in Textiles. *J. Am. Oil Chem. Soc.* **1982**, *59* (7), 322–327.
- (14) Malmsten, M.; Tiberg, F. Adsorption of Ethyl(hydroxyethyl) Cellulose on Polystyrene. *Langmuir* **1993**, *9* (4), 1098–1103.
- (15) Fu, Z.; Santore, M. M. Kinetics of Competitive Adsorption of PEO Chains with Different Molecular Weights. *Macromolecules* **1998**, *31*, 7014–7022.
- (16) Brandani, P.; Stroeve, P. Kinetics of Adsorption and Desorption of PEO-PPO-PEO Triblock Copolymers on a Self-Assembled Hydrophobic Surface. *Macromolecules* **2003**, *36*, 9502–9509.
- (17) Wu, C.; Liu, T.; White, H.; Chu, B. Atomic Force Microscopy Study of E99P69E99 Triblock Copolymer Chains on Silicon Surface. *Langmuir* **2000**, *16*, 656–661.
- (18) Marques, C.; Joanny, J. F.; Leibler, L. Adsorption of Block Copolymers in Selective Solvents. *Macromolecules* **1988**, *21*, 1051–1059.
- (19) Zhang, Q.; Archer, L. A. Interfacial Friction of Surfaces Grafted with One- and Two-Component Self-Assembled Monolayers. *Langmuir* **2005**, *21*, 5405–5413.
- (20) Carpick, R. W.; Dai, Q.; Ogletree, D. F.; Salmeron, M. Friction Force Microscopy Investigations of Potassium Halide Surfaces in Ultrahigh Vacuum: Structure, Friction and Surface Modification. *Tribol. Lett.* **1998**, *5* (1), 91–102.
- (21) Ruan, J.-A.; Bhushan, B. Atomic-Scale and Microscale Friction Studies of Graphite and Diamond Using Friction Force Microscopy. *J. Appl. Phys.* **1994**, *76* (9), 5022.
- (22) Sundararajan, S.; Bhushan, B. Static Friction and Surface Roughness Studies of Surface Micromachined Electrostatic Micro-motors Using an Atomic Force/Friction Force Microscope. *J. Vac. Sci. Technol., A* **2001**, *19* (4), 1777–1785.
- (23) Devaprakasham, D.; Khatri, O. P.; Shankar, N.; Biswas, S. K. Boundary Lubrication Additives for Aluminum: A Journey from Nano to Macro Tribology. *Tribol. Int.* **2005**, *38* (11–12), 1022–1034.
- (24) Bluhm, H.; Schwarz, U. D.; Meyer, K. P.; Wiesendanger, R. Anisotropy of Sliding Friction on the Triglycine Sulfate (010) Surface. *Appl. Phys. A: Mater. Sci. Process.* **1995**, *61* (5), 525–533.
- (25) Carpick, R. W.; Sasaki, D. Y.; Burns, A. R. Large Friction Anisotropy of a Polydiacetylene Monolayer. *Tribol. Lett.* **2000**, *7* (2–3), 79–85.
- (26) Marti, O.; Colchero, J.; Mlynek, J. Combined Scanning Force and Friction Microscopy of Mica. *Nanotechnology* **1990**, *1* (2), 141–144.
- (27) Bhushan, B.; Liu, H.; Hsu, S. M. Adhesion and Friction Studies of Silicon and Hydrophobic and Low Friction Films and Investigation of Scale Effects. *J. Tribol.* **2004**, *126* (3), 583–590.
- (28) Sasaki, N.; Kobayashi, K.; Tsukada, M. Atomic-Scale Friction Image of Graphite in Atomic-Force Microscopy. *Phys. Rev. B: Condens. Matter Mater. Phys.* **1996**, *54* (3), 2138–2149.
- (29) Behary, N.; El Achari, G. A.; Caze, C. Tribological Analysis of Glass Fibers Using Atomic Force Microscopy (AFM)/Lateral Force Microscopy (LFM). *J. Appl. Polym. Sci.* **2000**, *75* (8), 1013–1025.
- (30) Song, J.; Liang, J.; Liu, X.; Krause, W. E.; Hinestroza, J. P.; Rojas, O. J. Development and Characterization of Thin Polymer Films Relevant to Fiber Processing. *Thin Solid Films* **2009**, *517* (15), 4348–4354.
- (31) Gunnars, S.; Wagberg, L.; Cohen Stuart, M. A. Model Films of Cellulose: I. Method Development and Initial Results. *Cellulose* **2002**, *9* (3–4), 239–249.
- (32) Nisman, R.; Smith, P.; Vancso, G. J. Anisotropic Friction at the Surface of Lamellar Crystals of Poly(oxymethylene) by Lateral Force Microscopy. *Langmuir* **1994**, *10*, 1667–1669.
- (33) Diakova, B.; Kaisheva, M.; Platiikanov, D. Thin Liquid Films from Polyoxyethylene-Polyoxypropylene-Block Copolymer on the Surface of Fused Quartz. *Colloids Surf., A* **2001**, *190* (1–2), 61–70.
- (34) Liu, Y.; Evans, D. F.; Song, Q.; Grainger, D. W. Structure and Frictional Properties of Self-Assembled Surfactant Monolayers. *Langmuir* **1996**, *12*, 1235–1244.
- (35) Ruths, M.; Alcantar, N. A.; Israelachvili, J. N. Boundary Friction of Aromatic Silane Self-Assembled Monolayers Measured with the Surface Forces Apparatus and Friction Force Microscopy. *J. Phys. Chem. B* **2003**, *107*, 11149–11157.
- (36) Wong, J. S.; Granick, S. Open Questions about Polymer Friction. *J. Polym. Sci., Part B: Polym. Phys.* **2007**, *45* (24), 3237–3239.
- (37) Li, Y.; Liu, H.; Song, J.; Rojas, O. J.; Hinestroza, J. P. Adsorption and Association of a Symmetric PEO-PPO-PEO Triblock Copolymer on Polypropylene, Polyethylene, and Cellulose Surfaces. *ACS Appl. Mater. Interfaces* **2011**, *3*, 2349–2357.
- (38) Fu, Y.; Bai, S.; Cui, S.; Qiu, D.; Wang, Z.; Zhang, X. Hydrogen-Bonding-Directed Layer-by-Layer Multilayer Assembly: Reformation Yielding Microporous Films. *Macromolecules* **2002**, *35*, 9451–9458.
- (39) Wang, Y.; Ge, S.; Rafailovich, M.; Sokolov, J.; Zou, Y.; Ade, H.; Lüning, J.; Lustiger, A.; Maron, G. Crystallization in the Thin and Ultrathin Films of Poly(ethylene-vinyl acetate) and Linear Low-Density Polyethylene. *Macromolecules* **2004**, *37*, 3319–3327.
- (40) Zhang, F.; Baralia, G.; Boborodea, A.; Bailly, C.; Nysten, B.; Jonas, A. M. Partial Dewetting of Polyethylene Thin Films on Rough Silicon Dioxide Surfaces. *Langmuir* **2005**, *21*, 7427–7432.

- (41) Carlsson, C. M. G.; Stroem, G. Reduction and Oxidation of Cellulose Surfaces by Means of Cold Plasma. *Langmuir* **1991**, *7*, 2492–2497.
- (42) Wang, A.; Jiang, L.; Mao, G.; Liu, Y. Direct Force Measurement of Silicone- and Hydrocarbon-Based ABA Triblock Surfactants in Alcoholic Media by Atomic Force Microscopy. *J. Colloid Interface Sci.* **2002**, *256* (2), 331–340.
- (43) Zhang, Q.; Archer, L. A. Boundary Lubrication and Surface Mobility of Mixed Alkylsilane Self-Assembled Monolayers. *J. Phys. Chem. B* **2003**, *107*, 13123–13132.
- (44) Brown, H. R. Chain Pullout and Mobility Effects in Friction and Lubrication. *Science* **1994**, *263* (5152), 1411–1413.
- (45) Li, J.-T.; Caldwell, K. D.; Rapoport, N. Surface Properties of Pluronic-Coated Polymeric Colloids. *Langmuir* **1994**, *10*, 4475–4482.
- (46) Lee, S.; Iten, R.; Müller, M.; Spencer, N. D. Influence of Molecular Architecture on the Adsorption of Poly(ethylene oxide)–Poly(propylene oxide)–Poly(ethylene oxide) on PDMS Surfaces and Implications for Aqueous Lubrication. *Macromolecules* **2004**, *37*, 8349–8356.
- (47) Lee, S.; Müller, M.; Ratoi-Salagean, M.; Vörös, J.; Pasche, S.; De Paul, S. M.; Spikes, H. A.; Textor, M.; Spencer, N. D. Boundary Lubrication of Oxide Surfaces by Poly(L-lysine)-g-poly(ethylene glycol) (PLL-g-PEG) in Aqueous Media. *Tribol. Lett.* **2003**, *15* (3), 231–239.
- (48) Tada, T.; Kaneko, D.; Gong, J. P.; Kaneko, T.; Osada, Y. Surface Friction of Poly(dimethyl Siloxane) Gel and Its Transition Phenomenon. *Tribol. Lett.* **2004**, *17* (3), 505–511.
- (49) Dorris, G. M.; Gray, D. G. The Surface Analysis of Paper and Wood Fibers by ESCA - Electron Spectroscopy for Chemical Analysis—I. Applications to Cellulose and Lignin. *Cellulose Chem. Technol.* **1978**, *12*, 9–23.